LETTER

doi:10.1038/nature10820

Imaging ultrafast molecular dynamics with laser-induced electron diffraction

Cosmin I. Blaga[1], Junliang Xu[2], Anthony D. DiChiara[1], Emily Sistrunk[1], Kaikai Zhang[1], Pierre Agostini[1], Terry A. Miller[3], Louis F. DiMauro[1] & C. D. Lin[2]

Establishing the structure of molecules and solids has always had an essential role in physics, chemistry and biology. The methods of choice are X-ray and electron diffraction, which are routinely used to determine atomic positions with sub-ångström spatial resolution. Although both methods are currently limited to probing dynamics on timescales longer than a picosecond, the recent development of femtosecond sources of X-ray pulses and electron beams suggests that they might soon be capable of taking ultrafast snapshots of biological molecules[1,2] and condensed-phase systems[3–6] undergoing structural changes. The past decade has also witnessed the emergence of an alternative imaging approach based on laser-ionized bursts of coherent electron wave packets that self-interrogate the parent molecular structure[7–11]. Here we show that this phenomenon can indeed be exploited for laser-induced electron diffraction[10] (LIED), to image molecular structures with sub-ångström precision and exposure times of a few femtoseconds. We apply the method to oxygen and nitrogen molecules, which on strong-field ionization at three mid-infrared wavelengths (1.7, 2.0 and 2.3 μm) emit photoelectrons with a momentum distribution from which we extract diffraction patterns. The long wavelength is essential for achieving atomic-scale spatial resolution, and the wavelength variation is equivalent to taking snapshots at different times. We show that the method has the sensitivity to measure a 0.1 Å displacement in the oxygen bond length occurring in a time interval of ~5 fs, which establishes LIED as a promising approach for the imaging of gas-phase molecules with unprecedented spatio-temporal resolution.

In conventional electron diffraction (CED), an external multi-kilovolt beam impinges on a molecular gas sample[12–14], producing a diffraction pattern by means of elastic scattering. The electron's high energy promotes core-penetrating collisions (impact parameters $\leq$0.1 Å), in which the electron–molecule interaction is dominated by the strong short-range atomic-like potential while the bonding valence electrons look transparent. Conceptually, LIED is a time-resolved equivalent of CED. The field-ionized and accelerated coherent electron wave packet rescattering from its parent molecular core[10] (Fig. 1a) mimics the CED electron beam. If the rescattering wave packet is sufficiently energetic, the well-established bond length retrieval method of CED is applicable. We ensure that this is the case by using intense mid-infrared lasers for producing high-energy electron wave packets[15,16] (see Methods). We can then exploit theory that establishes that large-momentum-transfer backscattered electrons in LIED are equivalent in spatial resolution to those in CED[17], and use the LIED momentum angular distributions obtained at different wavelengths to observe changes in molecular bond lengths over an interval of a few femtoseconds.

The principle underpinning our approach is the strong-field rescattering model[18,19] (Fig. 1a), in which a molecule is first ionized by an intense low-frequency field that promotes an electronic wave packet into the continuum at time t_b. Approximately half of the electrons, dubbed direct (black dashed line in Fig. 1a), drift away from the vicinity of the molecule and are detected as low-momentum events. At a different t_b, the electron is accelerated by the laser field but follows a trajectory (magenta dashed line) that returns it to the core, where it can rescatter at time t_r. During the propagation time, $\Delta t = t_r - t_b$, the electron acquires significant kinetic energy from the field before rescattering. As the deBroglie wavelength of the returning wave packet becomes comparable to the molecular dimension, the interatomic spacing can be determined. At t_r the wave packet can either recombine to emit a high-energy photon[20,21] (high harmonic generation) or scatter, producing a far-field diffraction pattern. Both processes generate signals that convey structural information about the parent or target molecule, but only LIED provides a direct conceptual link to the CED method.

In contrast with CED's field-free scattering, LIED is a strong-field process; the laser's influence therefore needs to be removed to allow the extraction of field-free electron–ion differential cross-sections (DCS) from the measured LIED momentum distribution. The required deconvolution procedure is based on the quantitative rescattering theory[11,22,23], previously validated for various atoms and molecules[24–27]. It states that in the strong-field approximation, the detected momentum $\mathbf{p}$, shown in Fig. 1a for an unaligned N_2 distribution, is the vector sum of the momentum after recollision, $\mathbf{p}_r$, and the field's vector potential, $\mathbf{A}_r$, at the moment of rescattering, t_r. Electrons detected at various angles along the circumference defined at constant $|\mathbf{p}_r|$ (magenta dashed circle in Fig. 1a) thus constitute field-free DCS, equivalent to the DCS from CED. The DCS extracted according to this prescription from the experimentally determined momentum distribution for $|\mathbf{p}_r| = 2.71$ a.u. (atomic unit of linear momentum $= 1.99 \times 10^{-24}$ kg m s^{-1}) or 100-eV recollision energy is shown in Fig. 1b, and is found to agree well (within normalization constants) with the CED measurement[28] and our theoretical result. Consistent agreement is achieved for analysis at different laser wavelengths and intensities, and also for O_2. (Supplementary Information provides a detailed description of the DCS extraction procedure and a presentation of the factors that influence the interpretation of the LIED momentum distribution, for example the role of short and long trajectories, multiple returns, inelastic scattering and molecular excitations.)

When bond lengths are being extracted from CED measurements, molecules are treated as sets of independent atoms with fixed interatomic distances; chemical properties, such as molecular bonding, are neglected. The validity of this so-called independent atom model[12] (IAM) approach depends on the dominance of core-penetrating collisions facilitated by multi-keV electron beams. Within IAM and restricting our discussion to homonuclear diatomic molecules, the DCS for electrons colliding with unaligned molecules can be expressed as $\sigma_M = 2\sigma_A + 2\sigma_A \sin(qR)/qR$. The first term on the right is the contribution to the DCS from the incoherent sum of two atoms and conveys no structural information. The second is a molecular interference term depending explicitly on the internuclear distance R and the elastic momentum transfer

[1]Department of Physics, The Ohio State University, Columbus, Ohio 43210, USA. [2]Department of Physics, Kansas State University, Manhattan, Kansas 66506, USA. [3]Department of Chemistry, The Ohio State University, Columbus, Ohio 43210, USA.

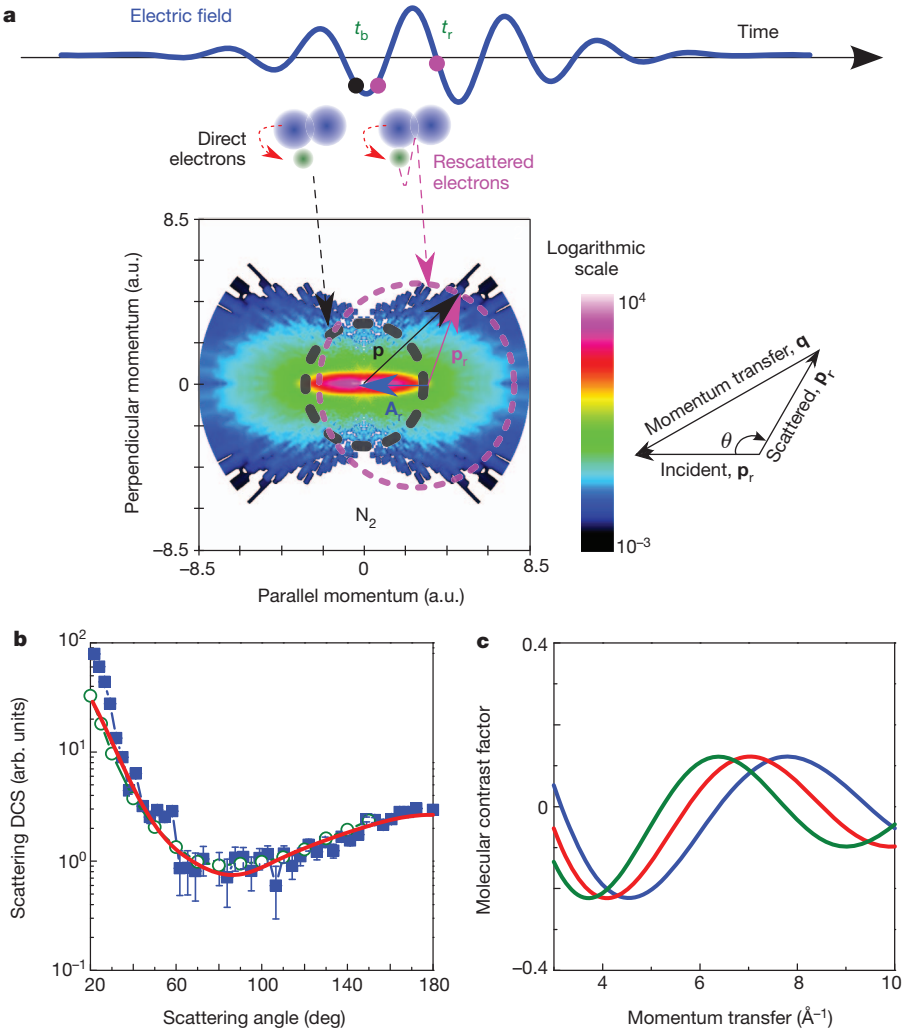

Figure 1 | The principle of laser-induced electron diffraction. **a**, Strong-field rescattering. An electron is released at time t_b in the electric field (solid blue line) of an intense mid-infrared laser. For certain initial times t_b, 'direct' electrons drift away from the core (solid blue), detected with momenta inside the dashed black circle. At other birth times, the electron returns roughly an optical cycle later back to the core (magenta trajectory). After elastic backscattering the electron gains additional momentum from the field, resulting in a larger detected momentum and separability from the direct ones (magenta dashed circle). A quasi-classical analysis allows one to deconstruct the detected momentum $\mathbf{p}$ into the momentum during rescattering $\mathbf{p}_r$, using the vector relationship $\mathbf{p} = \mathbf{p}_r - \mathbf{A}_r$ (atomic units), where $\mathbf{A}_r = (\mathbf{A})(t_r)$ is the field's vector potential at t_r. The inset defines the incident momentum $\mathbf{p}$, the scattered momentum $\mathbf{p}_r$, the rescattering angle θ and the momentum transfer $\mathbf{q}$. **b**, The DCS (blue solid squares) extracted from the N_2 distribution in **a** (260 TW cm^{-2}, 50 fs, 2.0 μm pulses) by sweeping the rescattering angle θ along the circumference of a circle of radius $|\mathbf{p}_r| = 2.71$ a.u. The error bars indicate the Poissonian uncertainty associated with the number of electrons detected at a given angle. The open green circles are data from CED measurements from ref. 28. The solid red line is calculated by using the independent atom model (IAM) for the CED data. At small scattering angles the LIED data are 'contaminated' by the direct electrons and are therefore not part of the analysis. **c**, Calculated MCFs plotted as a function of momentum transfer for three different N_2 bond distances: 0.99 Å (blue curve), 1.10 Å (red curve) and 1.21 Å (green curve). The plot shows that as the internuclear separation R is changed, the fringes shift from ~6 Å^{-1} to 8 Å^{-1}.

$q = 2p_r\sin(\theta/2)$, where θ is the scattering angle shown in Fig. 1a. Good spatial resolutions require large momentum transfers producing small interference terms. In CED it is convenient to define a molecular contrast factor (MCF) as the ratio of the second term to the first term. For typical q values of about 5–10 Å^{-1}, the MCF is ±0.15. With N_2 as an example, the method's spatial precision is emphasized by the extreme sensitivity of the MCF term to small changes in bond length, as shown in Fig. 1c by the clear shift in fringe maximum from 6 Å^{-1} to 8 Å^{-1} for 0.1-Å changes in R. This is a well-known benefit in precision of any interferometric measurement, such as the Young double-slit experiment. Therefore, for large momentum transfers, bond lengths can be extracted with the use of LIED by using similar principles to CED (see Supplementary Information). In our experiment, sufficiently energetic collisions are generated by exploiting the λ^2 scaling of the rescattering process at long wavelengths[15,16]. For instance, a 2.3-μm pulse results in an eightfold increase in rescattering energies over that achieved with a traditional 0.8-μm Ti:sapphire laser, yielding rescattering energies in excess of 200 eV. In addition, our LIED analysis is restricted to large-angle scattering, thus producing large momentum transfers, comparable in value to those of CED.

The dynamics of the rescattering process implies that, at constant $|\mathbf{p}_r|$, the time Δt between birth and rescattering of the electron wave packet is proportional to the laser optical cycle and hence the wavelength. Consequently, after ionization at t_b, the bond length begins adjusting to the new electronic configuration and thus at t_r the returning wave packet captures the diffraction image corresponding to a non-equilibrium internuclear distance. Thus, a series of images captured at different wavelengths equates to mapping the nuclear motion. If the electron removal is rapid, the Frank–Condon principle can be applied to evaluate the subsequent motion of the vibrational wave packet. We emphasize that Frank–Condon estimates are only approximate, because the impulsive nature of tunnel ionization is speculative. In this

study, the three mid-infrared wavelengths were, in principle, probing the internuclear separation 4–6 fs after tunnelling ionization.

The baseline for our LIED investigation was ionization of the highest occupied molecular orbital (HOMO) of N_2, the bonding σ_a orbital. Removal of the σ_a electron results in a small change in the equilibrium N–N distance from 1.10 Å (neutral) to 1.12 Å (ion)[29]. The experimental DCS (for example Fig. 1b) is matched to an IAM calculation by fitting the normalization constant and the internuclear separation so as to minimize the variance between experiment and theory (see Supplementary Information). Figure 2a shows the best-fit MCF (red line) retrieved from the 2-μm experiment (symbols), obtained with a N–N distance of 1.14 Å. Comparing CED data at the same collision energy (120 eV), we estimate a 0.05-Å error on the retrieved bond length. For comparison, we also plot in Fig. 2a the theoretical MCF calculated for N–N distances deviating from the fitted value by ±5 pm (dashed lines) and equal to that of neutral N_2 (dotted line). Figure 2c shows the analysis performed for a collision momentum of 4.11 a.u. (230 eV energy) using 2.3-μm pulses at 290 TW cm^{-2}. The retrieved N–N distance is 1.12 Å. In addition, LIED measurements performed at 1.7 μm result in a retrieved bond length of 1.15 Å. These three retrieved bond lengths are plotted in Fig. 2e as a function of time, using the classical correspondence with wavelength discussed above. The three retrieved bond lengths agree, within a 0.05-Å uncertainty, with the accepted N_2 equilibrium value. However, the experiment cannot resolve the small N–N bond motion (~0.02 Å) during the 4–6-fs time interval after tunnel ionization.

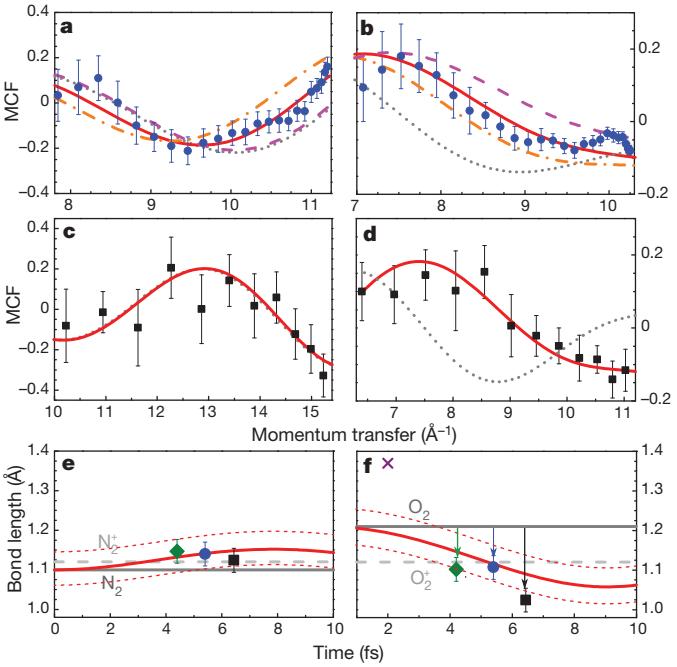

Figure 2 | LIED for unaligned N_2 and O_2 molecules. **a**–**d**, MCF extracted from the experimental data (scattered symbols) in comparison with theoretical predictions. The best-fit bond lengths are obtained by fitting the DCS extracted directly from the measurement (see Supplementary Information). The solid red line is the MCF calculated using the best-fit bond length. The dotted grey line is the MCF calculated using the equilibrium N_2 bond length. The dashed magenta and dash-dotted orange lines in **a** and **b** are the calculated MCFs using bond lengths that deviate by −5 and +5 pm, respectively, around the best fit. The error bars obey a Poisson statistical distribution. **a**, N_2 data taken with 260 TW cm^{-2}, 2.0 μm pulses (p_r = 2.97 a.u.). **c**, N_2 data taken with 290 TW cm^{-2}, 2.3 μm pulses (p_r = 4.11 a.u.). **b**, O_2 data taken with 133 TW cm^{-2}, 2.0 μm pulses (p_r = 2.91 a.u.). **d**, O_2 data taken with 150 TW cm^{-2}, 2.3 μm pulses (p_r = 2.97 a.u.). **e**, **f**, Illustration of bond change for N_2 (**e**) and O_2 (**f**) after ionization. The bond lengths extracted from the LIED measurements at each wavelength (squares, 2.3 μm; circles, 2 μm; diamonds, 1.7 μm) are shown. The associated error bars represent the IAM standard deviation resulting from experimental uncertainties. The time and wavelength correspondence is based on a classical analysis (see Supplementary Information). The red curves depict the evolution of the nuclear wave packet's centre (solid) and its associated full width at half-maximum (dotted), computed in the Frank–Condon approximation. The equilibrium bond lengths are indicated by the solid (neutral species) and dashed grey (ion) lines. For O_2, the vertical arrows indicate that the measured bond lengths for all three wavelengths are consistently shorter (~0.1 Å) than the equilibrium length for the neutral species and are statistically meaningful. The classical behaviour suggests that this is a consequence of the 4–6-fs bond evolution after ionization. The bond length reported in ref. 10 (purple cross) was extracted from a 0.8-μm laser experiment on aligned O_2 molecules. The short wavelength produced smaller return energies (<50 eV), thus complicating the interpretation and analysis of the momentum distribution, ultimately producing larger uncertainty in bond length.

In contrast to N_2, the O_2 HOMO is an anti-bonding π_a orbital, and ionization leads to a large change in the O–O equilibrium distance from 1.21 Å (neutral) to 1.10 Å (ion)[29]. By following the same procedure as outlined above, the extracted O–O distances for 1.7, 2.0 and 2.3-μm LIED measurements are 1.10, 1.11 and 1.02 Å, respectively. Figure 2b, d shows the MCF analysis at the last two wavelengths, again by comparing experimentally determined MCF values against the theoretical best fit, and against theoretical fits obtained for a bond length that differs from the best fit by ±5 pm or is equal to that of neutral O_2. In contrast to the N_2 experiments, the MCF curve calculated by using the neutral equilibrium distance does not fit the experiment at either wavelength. The O–O distances derived from the best fits deviate by 2–4 standard deviations from the equilibrium value, providing a high degree of confidence (>99.9%) that the bond has shortened in the 4–6-fs interval after ionization. The Frank–Condon curves in Fig. 2f show the free time evolution of the centre of the nuclear wave packet (O–O distance, solid red line), whereas dotted red lines indicate its width (full width at half-maximum). The three experimental data points in Fig. 2f show a statistically significant decrease (0.1 Å) in the O–O bond length from its initial, neutral equilibrium distance of 1.21 Å, as indicated by the vertical arrows. However, the spatial resolution of the experiment is insufficient to track the much smaller change in bond length (~0.05 Å resolution) occurring within the 4–6-fs time window spanned by the three measurement points. Regarding temporal resolution, we estimate an uncertainty of 2–3 fs in assigning a return time for each wavelength (see Supplementary Information).

Our findings illustrate that LIED can image sub-ångström structural changes in gas-phase molecules with femtosecond time resolution. We expect that the use of few-cycle pulses, bichromatic fields, additional wavelengths and improved counting rates will enhance the temporal resolution, and that the method can be used in pump-probe setups to interrogate molecules undergoing conformational transformations. A next step would be to apply LIED to more complex molecules, to aligned or oriented molecules, and to vibrationally or electronically excited molecules. Compared with a CED experiment, LIED's ability to control the returning electron wave packet coherently by means of bichromatic laser fields and/or ellipticity could open new paths in electron diffraction.

METHODS SUMMARY

Details of the laser system used in the experiment have been described previously[16]. In brief, an optical parametric amplifier (Topas-HE; LightConversion) pumped by a near-infrared Ti:sapphire front-end subsystem (0.8 μm, 4.4 mJ, 50 fs, 1 kHz) generates continuously tunable ultra-short (0.5 mJ, 50 fs) linearly polarized pulses from 1.2 to 2.3 μm. Angle-resolved (collection angle 1.6°) photoelectron energy distributions were recorded by focusing the laser in a ~22-cm field-free time-of-flight electron spectrometer. At each wavelength, the laser-driven diffraction image was obtained by rotating the laser polarization with respect to the spectrometer axis in steps of 2°, using zero-order half-wave plates. The sequence of collection angles was randomized to minimize systematic errors. For each angle, data were collected for about 10^6 laser shots, thus ensuring the necessary dynamic range while the count rate was kept below three hits per shot to minimize space-charge effects.

The energy calibration of the spectrometer was performed by recording the well-known above-threshold ionization (ATI) spectra of various noble gases with long (230-ps) pulses. The relative energy resolution $\Delta E/E$ of the apparatus was determined to be better than 1.4%, inferred from the long-lived Rydberg series present in the ATI spectrum of argon taken with 50-fs, 0.8-μm pulses. Finally, for each wavelength the peak intensities were estimated by analysing the $2U_p$ and $10U_p$ classical cutoffs present in the photoelectron energy distribution (see Supplementary Information for details). The cutoff values agree very well with numerical results based on single-active electron quantum calculations[16], and we estimate the accuracy of our technique to be within an error of 15%. These uncertainties were found to lead to 1–2-pm changes in the extracted bond lengths for all data sets.

Received 8 June; accepted 15 December 2011.

1. Seibert, M. M. *et al.* Single mimivirus particles intercepted and imaged with an X-ray laser. *Nature* **470,** 78–81 (2011).
2. Chapman, H. *et al.* Femtosecond X-ray protein nanocrystallography. *Nature* **470,** 73–77 (2011).
3. Zewail, A. H. & Thomas, J. M. *4D Electron Microscopy: Imaging in Space and Time* (Imperial College Press, 2010).
4. Eichberger, M. *et al.* Snapshots of cooperative atomic motions in the optical suppression of charge density waves. *Nature* **468,** 799–802 (2010).
5. Sciaini, G. & Miller, D. Femtosecond electron diffraction: heralding the era of atomically resolved dynamics. *Rep. Prog. Phys.* **74,** 096101 (2011).
6. Elsaesser, T. & Woerner, M. Photoinduced structural dynamics of polar solids studied by femtosecond X-ray diffraction. *Acta Crystallogr. A* **66,** 168–178 (2010).
7. Niikura, H. *et al.* Sub-laser-cycle electron pulses for probing molecular dynamics. *Nature* **417,** 917–922 (2002).
8. Itatani, J. *et al.* Tomographic imaging of molecular orbitals. *Nature* **432,** 867–871 (2004).
9. Li, W. *et al.* Time-resolved dynamics in N_2O_4 probed using high harmonic generation. *Science* **322,** 1207–1211 (2008).
10. Meckel, M. *et al.* Laser-induced electron tunneling and diffraction. *Science* **320,** 1478–1482 (2008).
11. Lin, C. D., Le, A. T., Chen, Z., Morishita, T. & Lucchese, R. Strong-field rescattering physics—self-imaging of a molecule by its own electrons. *J. Phys. B* **43,** 122001 (2010).
12. Hargittai, I&. Hargittai, M. (eds) *Stereochemical Applications of Gas-Phase Electron Diffraction* (VCH, 1998).
13. Reckenthaeler, P. *et al.* Time-resolved electron diffraction from selectively aligned molecules. *Phys. Rev. Lett.* **102,** 213001 (2009).
14. Zewail, A. H. Femtochemistry: atomic-scale dynamics of the chemical bond using ultrafast lasers. *Angew. Chem. Int. Ed.* **39,** 2586–2631 (2000).
15. Tate, J. *et al.* Scaling of wave-packet dynamics in an intense midinfrared field. *Phys. Rev. Lett.* **98,** 013901 (2007).
16. Colosimo, P. *et al.* Scaling strong-field interactions towards the classical limit. *Nature Phys.* **4,** 386–389 (2008).
17. Xu, J., Chen, Z., Le, A. T. & Lin, C. D. Self-imaging of molecules from diffraction spectra by laser-induced rescattering electrons. *Phys. Rev. A* **82,** 033403 (2010).
18. Schafer, K. J., Yang, B., DiMauro, L. F. & Kulander, K. C. Above threshold ionization beyond the high harmonic cutoff. *Phys. Rev. Lett.* **70,** 1599–1602 (1993).
19. Corkum, P. B. Plasma perspective on strong field multiphoton ionization. *Phys. Rev. Lett.* **71,** 1994–1997 (1993).
20. Baker, S. *et al.* Probing proton dynamics in molecules on an attosecond time scale. *Science* **312,** 424–427 (2006).
21. Torres, R. *et al.* Revealing molecular structure and dynamics through high-order harmonic generation driven by mid-IR fields. *Phys. Rev. A* 81**,** 051802(R), http://dx.doi.org/10.1103/PhysRevA.81.051802 (2010).
22. Morishita, T., Le, A. T., Chen, Z. & Lin, C. D. Accurate retrieval of structural information from laser-induced photoelectron and high-order harmonic spectra by few-cycle laser pulses. *Phys. Rev. Lett.* **100,** 013903 (2008).
23. Chen, Z., Le, A. T., Morishita, T. & Lin, C. D. Quantitative rescattering theory for laser-induced high-energy plateau photoelectron spectra. *Phys. Rev. A* **79,** 033409 (2009).
24. Ray, D. *et al.* Large-angle electron diffraction structure in laser-induced rescattering from rare gases. *Phys. Rev. Lett.* **100,** 143002 (2008).
25. Okunishi, M. *et al.* Experimental retrieval of target structure information from laser-induced rescattered photoelectron momentum distributions. *Phys. Rev. Lett.* **100,** 143001 (2008).
26. Okunishi, M., Niikura, H., Lucchese, R. R., Morishita, T. & Ueda, K. Extracting electron-ion differential scattering cross sections for partially aligned molecules by laser-induced rescattering photoelectron spectroscopy. *Phys. Rev. Lett.* **106,** 063001 (2011).
27. Cornaggia, C. Electron-ion elastic scattering in molecules probed by laser-induced ionization. *J. Phys. B* **42,** 161002 (2009).
28. Dubois, R. D. & Rudd, M. E. Differential cross sections for elastic scattering of electrons from argon, neon, nitrogen and carbon monoxide. *J. Phys. B* **9,** 2657–2667 (1976).
29. Dekock, R. L. & Gray, H. B. *Chemical Structure and Bonding* 229 (University Science Books, 1989).

Supplementary Information is linked to the online version of the paper at www.nature.com/nature.

Acknowledgements The work at The Ohio State University and Kansas State University was performed under DOE/BES contracts DE-FG02-06ER15833 and DE-FG02-06ER15832, respectively. L.F.D. acknowledges support from the Hagenlocker chair.

Author Contributions C.I.B. and J.X. designed the experiment and performed the data analysis. C.I.B., A.D.D., E.S. and K.Z. performed the experiment. J.X. and C.D.L. performed the theoretical analysis. C.I.B., J.X., A.D.D., P.A., T.A.M., L.F.D. and C.D.L. interpreted the results and prepared the manuscript.

Author Information Reprints and permissions information is available at www.nature.com/reprints. The authors declare no competing financial interests. Readers are welcome to comment on the online version of this article at www.nature.com/nature. Correspondence and requests for materials should be addressed to C.I.B. (cblaga@mps.ohio-state.edu).